

Photocatalytic Reduction of Nicotinamide Co-factor by Perylene Sensitized Rh^{III} Complexes**

Jannik Brückmann^{+, [a]}, Carolin Müller^{+, [b, c]}, Ilse Friedländer,^[b] Alexander K. Mengele,^[a] Kalina Peneva,^[d, e] Benjamin Dietzek-Ivanšić,^{*, [b, c, e]} and Sven Rau^{*, [a]}

Abstract: The ambitious goal of artificial photosynthesis is to develop active systems that mimic nature and use light to split water into hydrogen and oxygen. Intramolecular design concepts are particularly promising. Herein, we firstly present an intramolecular photocatalyst integrating a perylene-based light-harvesting moiety and a catalytic rhodium center

(Rh^{III}phenPer). The excited-state dynamics were investigated by means of steady-state and time-resolved absorption and emission spectroscopy. The studies reveal that photoexcitation of Rh^{III}phenPer yields the formation of a charge-separated intermediate, namely Rh^{III}phenPer^{*+}, that results in a catalytically active species in the presence of protons.

Introduction

Artificial photosynthesis aims to develop photocatalytic systems for light-driven water splitting.^[1] Promising structures are molecular assemblies combining a light-harvesting and a redox-active catalytic unit, which are chemically linked by a molecular bridge.^[2] Such molecularly defined systems offer the opportunity for detailed, mechanistic investigations upon structural modifications. From various studies, transition metal complexes, that is, based on Ru^{II}, Ir^{III}, Os^{II} or Re^I emerged as efficient photosensitizer building-blocks.^[2,3] However, to strive for sustainable photocatalysis it is mandatory to replace noble-metal sensitizers by low-cost and easy to derivatize organic chromophores such as oligothiophene^[4,5] and rylene^[6,7] dyes.

Due to their electron-deficiency perylene monoimide (PMI) and perylene diimides (PDI) often serve as sensitizers in oxidative catalysis^[8–10] but light-driven hydrogen evolution has recently been described as well.^[11] In addition, a few reports exist focussing on the use of rylene chromophores in intramolecular dyads for light-driven reduction reactions. For instance, Wasielewski *et al.*^[12,13] studied the impact of PMI and

PDI as well as naphthalene-imide chromophores coupled to Re^I and Mn^I-based carbon dioxide reduction catalysts. Peneva *et al.* described the integration of an [FeFe]-hydrogenase cluster into perylene based photosensitizers.^[14]

Here, we present the synthesis and spectroscopic studies of a novel photocatalyst dyad employing a perylene (Per) photosensitizer (phenPer = 5-(perylene-3-yl)-1,10-phenanthro-line) and ac RhCp* catalyst moiety, namely Rh^{III}phenPer ((phenPer)Rh(Cp*)Cl)Cl, see Figure 1). A number of previous studies report on the incorporation of [(N^N)Rh(Cp*)Cl]⁺ units (N^N = phen (1,10-phenanthroline) or bpy (2,2'-bipyridine)) in heterogeneous or homogenous catalytic systems.^[15,16] In contrast, only a few examples reveal intramolecular assemblies of RhCp*, that is, with a Ru^{II} polypyridine sensitizer^[17,18] or organic chromophores.^[19] However, an optimized linkage between the Ru^{II} polypyridine sensitizer and the RhCp* unit in some of these investigated dinuclear assemblies even allowed to surpass the rate of classical chemical catalysis at the Rh center when using these systems under photocatalytic conditions.^[20] Consequently, to unravel the light-induced processes in Rh^{III}phenPer we applied steady-state and transient absorption spectroscopy. In

[a] J. Brückmann,⁺ Dr. A. K. Mengele, Prof. S. Rau
Institute of Inorganic Chemistry I, Ulm University
Albert-Einstein-Allee 11, 89081, Ulm (Germany)
E-mail: sven.rau@uni-ulm.de
Homepage: <https://www.uni-ulm.de/en/nawi/nawi-anorg1/>

[b] Dr. C. Müller,⁺ I. Friedländer, Prof. B. Dietzek-Ivanšić
Institute of Physical Chemistry
Friedrich Schiller University Jena
Helmholtzweg 4, 07743 Jena (Germany)
E-mail: benjamin.dietzek@uni-jena.de
Homepage: <https://www.ipc.uni-jena.de/en/agdietzek>

[c] Dr. C. Müller,⁺ Prof. B. Dietzek-Ivanšić
Research Department Functional Interfaces
Leibniz Institute of Photonic Technology Jena
Albert-Einstein-Straße 9, 07745 Jena (Germany)

[d] Prof. K. Peneva
Institute of Organic Chemistry and Macromolecular Chemistry
Friedrich Schiller University Jena
Lessingstraße 8, 07743 Jena (Germany)

[e] Prof. K. Peneva, Prof. B. Dietzek-Ivanšić
Center for Energy and Environmental Chemistry Jena (CEEC Jena)
Friedrich Schiller University Jena
Philosophenweg 7a, 07743 Jena (Germany)

[*] These authors contributed equally.

[**] A previous version of this manuscript has been deposited on a preprint server (<https://doi.org/10.26434/chemrxiv-2021-g9bfz>).

 Supporting information for this article is available on the WWW under <https://doi.org/10.1002/chem.202201931>

 © 2022 The Authors. Chemistry - A European Journal published by Wiley-VCH GmbH. This is an open access article under the terms of the Creative Commons Attribution Non-Commercial NoDerivs License, which permits use and distribution in any medium, provided the original work is properly cited, the use is non-commercial and no modifications or adaptations are made.

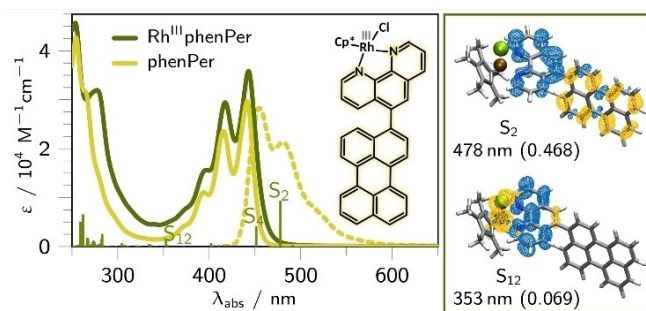


Figure 1. Extinction coefficients of $\text{Rh}^{\text{III}}\text{phenPer}$ (green) and phenPer (gold) and emission spectrum of phenPer (scaled relative to the absorption maximum) in acetonitrile. Structural formula of $\text{Rh}^{\text{III}}\text{phenPer}$ photocatalyst, highlighting the phenPer ligand in gold. Charge density differences of two selected optical transitions of $\text{Rh}^{\text{III}}\text{phenPer}$ (excitation occurs from yellow to blue). The respective TD-DFT simulated vertical transition energies and oscillator strengths are represented as green bars in the absorption spectrum (see also Table S2).

addition, the principal applicability of $\text{Rh}^{\text{III}}\text{phenPer}$ as a thermal and light-driven reduction catalyst for regioselective NAD^+ (nicotinamide adenine dinucleotide) hydrogenation forming NADH was investigated, guided by the question whether also in the case of $\text{Rh}^{\text{III}}\text{phenPer}$ chemical catalysis can be surpassed by a light-driven process.

Results and Discussion

Electrochemistry

To assist the interpretation of the photophysical properties, cyclic voltammograms (CVs) of phenPer and $\text{Rh}^{\text{III}}\text{phenPer}$ were collected. For solubility reasons the CV of phenPer is recorded in dichloromethane (see Figures S8–S10 and Table S1), while the CV of $\text{Rh}^{\text{III}}\text{phenPer}$ is monitored in acetonitrile. Generally, the orbitals involved in the first oxidation (highest occupied molecular orbital, HOMO) and reduction (lowest unoccupied molecular orbital, LUMO) are the orbitals involved in the lowest lying $\pi\pi^*$ absorption. The CVs of $\text{Per}^{\text{[21]}}$ and phenPer show the first oxidation at the Per -moiety (HOMO: π_{Per} -orbital) which is manifested in reversible oxidation waves at 0.55 V and 0.60 V vs. $\text{Fc}^{0/+}$, respectively. Also, the first reduction of both chromophores occurs at the Per -moiety (LUMO: π_{Per}^* -orbital) showing a reversible reduction wave at -2.17 and -2.15 V vs. $\text{Fc}^{0/+}$, respectively.^[21]

The CV of $\text{Rh}^{\text{III}}\text{phenPer}$ shows an oxidation wave at 0.52 V vs. $\text{Fc}^{0/+}$, which can be ascribed to the Per unit by comparison to Per and phenPer . In contrast to the phenPer ligand, this process is quasi-reversible, which presumably stems from an overlay of a reversible π_{Per} -centered oxidation with an irreversible oxidation of the chloride ions in solution.^[17,22] This oxidation wave is cathodically shifted with respect to phenPer , indicating a destabilization of the π_{Per} -orbitals in $\text{Rh}^{\text{III}}\text{phenPer}$ compared to phenPer .

The CV of $\text{Rh}^{\text{III}}\text{phenPer}$ reveals two quasi-reversible (-1.19 and -2.06 V vs. $\text{Fc}^{0/+}$) and three irreversible (-2.52 , -2.65 and -2.77 V vs. $\text{Fc}^{0/+}$) reduction peaks (see Figure S9). The individual reductions are localized on the Rh-ion (d-orbital) as well as on the phen- and Per -moiety (π^* -orbitals) of the phenPer ligand. In contrast to phenPer , the LUMO of $\text{Rh}^{\text{III}}\text{phenPer}$ is a Rh d-orbital. Thus, the first reduction (-1.19 V vs. $\text{Fc}^{0/+}$) is ascribed to a Rh-centered reduction, which is a two-electron $\text{Rh}^{\text{III/I}}$ process accompanied by a loss of the chlorido ligand ultimately forming $[(\text{phenPer})\text{Rh}^{\text{I}}(\text{Cp}^*)]$ ($\text{Rh}^{\text{phenPer}}$).^[17]

The second reduction at -2.06 V vs. $\text{Fc}^{0/+}$ is associated with the Per -moiety (π_{Per}^* -orbital). This reduction is anodically shifted with respect to Per and phenPer , due to the increased electron density, that is, the coordination of the Rh^{I} ion. At more cathodic potentials between -2.5 and -2.8 V vs. $\text{Fc}^{0/+}$, the phen- and Per -moiety are reduced irreversibly.

Ground state absorption and emission properties

It is essential to understand the nature of the initially excited states to rationalize the photochemical processes underlying light-driven catalysis. Figure 1 shows the ground state absorption spectra of phenPer and $\text{Rh}^{\text{III}}\text{phenPer}$ in acetonitrile.

The absorption spectrum of $\text{Rh}^{\text{III}}\text{phenPer}$ shows a strong absorption band between 200 and 300 nm and a vibrationally resolved absorption feature between 350 and 500 nm. By direct comparison to the absorption of $[(\text{phen})\text{Rh}^{\text{III}}(\text{Cp}^*)\text{Cl}]\text{Cl}$ (see Figure S25), the absorption band centered at 320 nm is assigned to MLCT and $\pi\pi^*$ transitions on the phen sphere (see S_{12} and S_{35} in Table S2). The visible absorption band of $\text{Rh}^{\text{III}}\text{phenPer}$ shows maxima at 442 nm (2.80 eV, $3.4 \times 10^4 \text{ M}^{-1} \text{ cm}^{-1}$), 415 nm (2.99 eV), 390 nm (3.19 eV) and 363 nm (3.42 eV) corresponding to Per -based (0,0), (0,1), (0,2) and (0,3) $S_0 \rightarrow S_1$ $\pi\pi^*$ transitions (see Figure S12).^[23] Similar $\pi\pi^*$ absorption bands are observed for phenPer (at 440 nm ($2.9 \times 10^4 \text{ M}^{-1} \text{ cm}^{-1}$), 415 nm, 393 nm and 373 nm) and Per (maxima at 444 nm ($3.2 \times 10^4 \text{ M}^{-1} \text{ cm}^{-1}$), 418 nm and 396 nm),^[24] indicating that the Per donor and Rh^{III} acceptor group are electronically decoupled in $\text{Rh}^{\text{III}}\text{phenPer}$. This is supported by DFT predicting a dihedral angle between the Per and phen moiety of 80° (see Tables S2 and S3).

PhenPer shows vibrationally resolved emission between 430 and 550 nm (see Figure 1) originating from the $S_1 \rightarrow S_0$ transition on the Per unit (see Figure S13).^[25] The features of phenPer are red-shifted (by 0.1 eV) compared to Per , due to the π -extension by the phen-unit (see CDDs in Table S3). The charge-transfer character of the S_1 state in phenPer also reduces the fluorescence quantum yield in phenPer (53%) with respect to Per (98%).^[26] Upon coordination of Rh^{III} to phenPer the perylene emission is quenched entirely, hinting to excited-state electron transfer towards the metal center. This is consistent with previous findings on $\text{Ru}^{\text{II}}\text{Rh}^{\text{III}}$ molecular dyads or polymeric Rh^{III} architectures.^[17,19] Likewise, addition of the sacrificial electron donor triethylamine (TEA) quenches the emission of phenPer (dynamic and static quenching, Stern-Volmer constants of 10^3 M^{-2} (I_0/I) and 2.5 M^{-1} (τ_0/τ), see

Figure S16). Hence, **phenPer** is capable of being photochemically reduced.

Photoinduced dynamics

To characterize the ultrafast photoinduced processes, femto-second transient absorption (fs-TA) spectra of **Rh^{III}phenPer** and **phenPer** were collected upon excitation at 400 nm (see Figures 2, S17 and S18) in acetonitrile and toluene, respectively. The impact of the solvent polarity (acetonitrile: $\epsilon=37.5$ and toluene: $\epsilon=2.4$) on the ultrafast processes was probed, to resolve the contributions of excited $\pi\pi^*$ and charge-separated states. The discussion starts with the TA data of **phenPer**, recorded as benchmark, and subsequently turns to the respective Rh-complex.

The TA spectra of **phenPer** in toluene closely resemble them of **Per**^[27], showing strong excited state absorption (ESA) centered at 725 nm (**Per**-centered $\pi\pi^*$ transitions^[27]) accompanied by ground state bleach (GSB) at 435 nm and stimulated emission (SE) features at 474 and 515 nm (see Figure S17).^[28,29] The agreement of the data derived here with data reported for **Per** and derived systems^[23,27,30] points to a photoinduced dynamics that primarily involves the **Per**-moiety of **phenPer**. Also, the TA spectra of **phenPer** in acetonitrile show the (GSB, SE and ESA) features typically observed for **Per**. However, the ESA band in acetonitrile ($\lambda_{\text{max}}=706$ nm, FWHM=0.25 eV) is blue-shifted and spectrally broadened compared to that in toluene ($\lambda_{\text{max}}=725$ nm, FWHM=0.12 eV). In addition, the ratio between the GSB to SE signals is higher in acetonitrile (*circa* 2.0) than toluene (*circa* 1.2). We associate this with the population of a charge transfer state in acetonitrile, where the excess electron density is delocalized on the phen- and **Per**-moiety of **phenPer**. This seems plausible, since such a (polar) charge-transfer state is energetically more stabilized in acetonitrile than

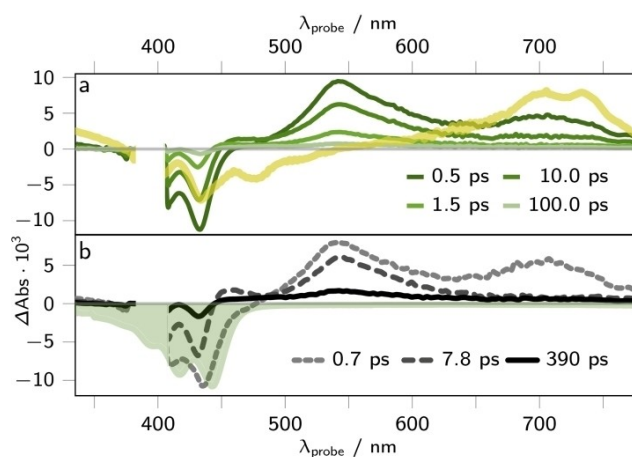


Figure 2. a) Transient absorption and b) decay associated spectra of **Rh^{III}phenPer** in acetonitrile upon 400 nm excitation. For reasons of comparability the scaled long-lived TA spectrum of **phenPer** (lifetime of 2.1 ns) collected at 400 nm excitation (excitation density of *circa* 5%) in acetonitrile is depicted in gold (a). The scaled inverted ground state absorption spectrum is shown in panel b (filled, green curve).

in toluene. With respect to the TA signals in toluene, the population of a charge transfer state causes the rise of additional ESA features (*e.g.*, phen-centered $\pi\pi^*$) and the decrease of SE from the **Per**-centered $\pi\pi^*$ sphere in acetonitrile.

Global kinetic analysis of the TA data in acetonitrile and toluene reveals three characteristic time-constants describing the decay of the signals, namely, $\tau_1=(0.5\pm 0.1)$ ps, $\tau_2=(111\pm 40)$ ps and $\tau_3=(3.1\pm 0.1)$ ns in toluene, and $\tau_1=(1.7\pm 0.3)$ ps, $\tau_2=(68\pm 5)$ ps and $\tau_3=(2.9\pm 0.2)$ ns in acetonitrile (see Figure S17). In agreement with literature reports on **Per**, we associate τ_1 with the population of the S_1 state via internal conversion and vibrational cooling,^[31] which is centered on the **Per**-moiety in toluene and delocalized on the **phenPer** chromophore in acetonitrile. Subsequently, the system relaxes back to the ground state with $\tau_3\approx 3$ ns, which agrees with the emission lifetime of **phenPer** in acetonitrile ($\tau_{\text{em}}=2.9$ ns, see Figure S15). The decrease of the excited state lifetime compared to **Per** (*circa* 4 ns^[32]) can be rationalized by the presence of additional deactivation-channels in **phenPer** (*e.g.*, rotation around the bond between the phen and **Per** unit), which we associate with τ_2 .

The TA spectrum of **Rh^{III}phenPer** recorded at a pump-probe delay of 0.5 ps in toluene or acetonitrile shows the characteristic $S_1\rightarrow S_n$ $\pi\pi^*$ absorption of ***Per** between 700 and 730 nm.^[27] These features are accompanied by GSB at 435 nm and SE at 475 nm. This indicates the population of states with excess electron density on the **Per**- (toluene) or **phenPer**-moiety (acetonitrile), in accordance with the findings for **phenPer**. However, the initial TA spectrum of **Rh^{III}phenPer** ($\Delta t=0.5$ ps) additionally reveals ESA centered at 540 nm (see Figure 2), which is typically associated with a **Per**-centered radical cation (**Per^{•+}**).^[33,34] Since, this ESA dominates the TA signals in acetonitrile but is less-pronounced in toluene compared to the ***Per** ESA (see Figure S18), the 540 nm feature hints to the population of a charge-separated state (see Figures 2 and S18). We associate the existence of both, ***Per** and **Per^{•+}** signatures in the initial TA spectrum with the excitation of different conformers, assuming conformational isomer-dependent oscillator strengths for $\pi\pi^*$ and ILCT transitions.

In toluene, the 540 nm signals, which are associated with a charge-separated species (**Rh^{III}phen[•]Per^{•+}**), vanish within 40 ps after optical excitation. The resulting spectrum of the long-lived species closely resembles the one of the **phenPer** ligand (*cf.* solid, black lines in Figures S17b and S18b), indicating the formation of a **Per**-centered state. Global analysis yields three characteristic time-constants in toluene, that is, $\tau_1=(2.3\pm 0.7)$ ps, $\tau_2=(40\pm 9)$ ps and $\tau_3=(4.8\pm 0.1)$ ns. We associate τ_1 with vibrational cooling populating the lowest-lying $\pi\pi^*_{\text{Per}}$ and ILCT states. With τ_2 the ILCT state decays back to the ground state, which is reflected in partial GSB recovery and the decay of the 540 nm signals. The so formed **Per**-centered $\pi\pi^*$ state non-radiatively decays back to the ground state with τ_3 (see model sketch in Figure S18).

Global lifetime analysis of the TA signals of **Rh^{III}phenPer** in acetonitrile yields $\tau_1=(0.6\pm 0.1)$ ps, $\tau_2=(6.9\pm 2.5)$ ps, $\tau_3=(280\pm 150)$ ps and $\tau_4=(47\pm 20)$ ps (see Figures 2 and S18).

The respective target model (used in the optimization routine) is shown in Figure 3.

Within the first 0.6 ps ($\tau_1 = 0.6 \pm 0.1$ ps) the characteristic *Per ESA and *Per SE at around 475 nm vanish, accompanied by the rise of ESA at around 480 nm (plateau). We ascribe the latter ESA to $\pi\pi^*$ transitions on a formally reduced phen-moiety (phen $^{\bullet-}$).^[35–37] Such a fast (< 1 ps) charge separation can be rationalized by the comparably high excited state oxidation potential $E(\text{Per}^{\bullet+}/^*\text{Per})$ of **Per** (–2.27 V) and **phenPer** (–2.13 V), respectively (see Figure S11 and Table S1). Consistent with our findings, literature reports similar rates (0.1 up to 1.5 ps) for the formation of a rylene radical cation^[38] or anion^[9,10] in PDI substituted systems.

The phen-centered intra-ligand charge-separated state decays via ligand-to-metal charge transfer (LMCT) with $\tau_2 = 6.9 \pm 2.5$ ps forming the fully charge-separated (CS) species $[(\text{phenPer}^{\bullet+})\text{Rh}^{\text{II}}(\text{Cp}^*\text{Cl})]^+$. This is reflected in the decay of ESA at around 480 nm ($\pi\pi^*_{\text{phen}^{\bullet-}}$). The CS species decays with 280 ± 150 ps (τ_3). In parallel to the charge-transfer cascade, the remaining fraction of the population of the ILCT state relaxes back to the ground state with $\tau_4 = 47 \pm 20$ ps (see Figure 3).

The decreased excited state lifetime of **Rh^{III}phenPer** (reduced by a factor of 8 compared to **phenPer**), further corroborates charge transfer from the **Per** moiety towards the Rh center. This is also reflected in the emission quenching upon coordination of **phenPer** to Rh^{III} (see Figure S14). In comparison to hybrid rylene imide transition metal complex architectures reported earlier, that show charge recombination of their radical anions^[10] or cations^[38] on the sub-100 ps timescale, the herein studied $[(\text{phenPer}^{\bullet+})\text{Rh}^{\text{II}}(\text{Cp}^*\text{Cl})]^+$ reveals an enhanced CS state lifetime. In contrast, the CS state of the structurally related, dinuclear transition metal complex $[(\text{tbbpy})_2\text{Ru}(\text{tpphz})\text{Rh}(\text{Cp}^*\text{Cl})]^{3+}$ (**Ru^{II}-tpphz-Rh^{III}**, tpphz: tetrapyrido[3,2-a:2',3'-c:3'',2''-h:2''',3'''-j]phenazine, tbbpy: 4,4'-di-*tert*-butyl-2,2'-bipyridine) is long-lived (> 2 ns^[18]) compared to the CS state of **Rh^{III}phenPer**, which can be rationalized by the comparably short charge separation distance in the latter.

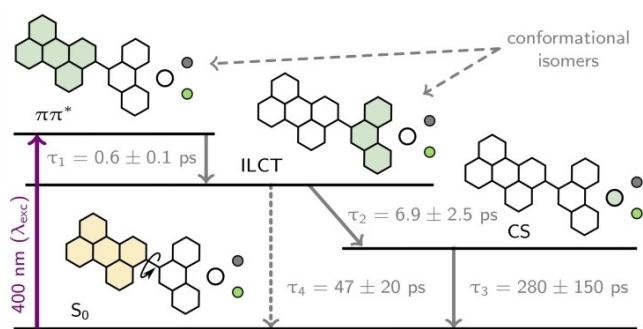


Figure 3. The Jablonski diagram shows the excited state dynamics of **Rh^{III}phenPer** upon photoexcitation at 400 nm in acetonitrile. The colours in the ground-state structure indicate the origin of the of the optically accessible $\pi\pi^*$ and ILCT states (yellow). The excess electron density in the excited states is highlighted in green.

Formation of the catalytically active species and redox catalysis

The formation of a two-fold reduced Rh^I species is key to the overall performance of the Rh^{III}-catalysts.^[17,18] To get insights into the reductive catalyst activation, the two-fold reduced catalyst (**Rh^IphenPer**) was selectively generated via the three following pathways: i) chemical reduction of the Rh^{III} center by a formate-driven thermal reaction^[39] (see Figure S19), ii) electrochemical reduction (see Figure S25), and iii) photochemical reduction upon LED-illumination in the presence of triethylamine (TEA) as sacrificial electron donor (see Figure S21). The in situ spectra obtained via those three methods are qualitatively identical (see Figure S25) and indicate the formation of **Rh^IphenPer**. This is revealed in the rise of a characteristic absorption band at 695 nm, which is assigned to Rh^I→phen MLCT transitions.^[18,40]

To evaluate the capability of **Rh^IphenPer** to drive the hydrogenation of NAD⁺,^[41] the increase in absorbance at 340 nm associated with $\pi\pi^*$ transitions of NADH, was monitored in situ.^[42] Those studies reveal the successful reduction of NAD⁺ to NADH at a constant turnover frequency (see Figures S26–S30). The chemical reduction, i.e., formate-driven activation of the catalyst serves as a well-understood benchmark for evaluation of a catalytically competent Rh(Cp*) sphere.^[17] In this setting, a turnover number of *circa* 30 (75% conversion) is obtained during an overall reaction time of 70 minutes at 40 °C which is about three times lower at room temperature (see Figures S26 and S27).

In addition, **Rh^{III}phenPer** shows light-driven catalytic activity. Upon 70 minutes of LED illumination at 400 nm (14 mWcm⁻²) or 470 nm (45 mWcm⁻²), respectively, an average turnover number of *circa* 4 (10% conversion) is found at room temperature (see Figures 4 and S28–S30). Increasing the temperature to 40 °C yields a TON of 4 or 7 upon illumination at 400 or 470 nm for 70 minutes, respectively. The absence of the absorption band at *ca.* 695 nm during photoredox catalysis

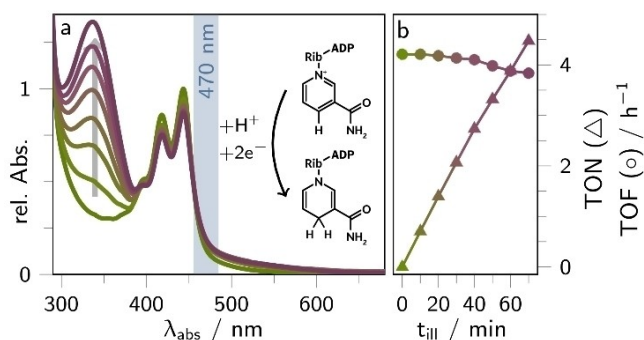


Figure 4. a) Normalized absorption spectrum of **Rh^{III}phenPer** (green, 5 μM) and upon LED-illumination at 470 nm (at room temperature for 70 minutes in steps of 10 minutes) in water:acetonitrile mixture (4:1, v:v) in the presence of phosphate-buffered (NaH_2PO_4 , 0.1 M) triethylamine (TEA, 0.12 M) and NAD^+ (0.2 mM). The increase in absorbance at around 340 nm reflects the catalytic conversion of NAD^+ to NADH, which is further reflected in b) the turnover number (TON, Δ) and turnover frequency (TOF, \circ) as shown in panel b.

reveals that accumulation of non-protonated and thus hydride transfer inactive $\text{Rh}^{\text{I}}\text{phenPer}$ does not occur. This was associated with the presence of NAD^+ in the catalytic mixture which seems to influence the subsequent protonation step as in absence of NAD^+ the characteristic $\text{Rh}^{\text{I}} \rightarrow \text{phen}$ MLCT transitions are observed (see Figures S20 and S23). Thus, during photocatalysis, $\text{Rh}^{\text{I}}\text{phenPer}$ is efficiently protonated giving rise to the hydride transfer active $[(\text{phenPer})\text{Rh}^{\text{III}}(\text{Cp}^*)\text{H}]^+$ species ($\text{Rh}^{\text{III}}\text{HphenPer}$) or its tautomerized form $[(\text{phenPer})\text{Rh}^{\text{III}}(\text{Cp}^*\text{H})]^+$, respectively.^[39,43] It should be noted that recent theoretical studies of the hydride transfer onto NAD^+ revealed, that the classical metal-hydride species rather than the thermodynamically more stable tautomerized form is the active hydride transfer reagent,^[44] during hydride transfer NAD^+ is arranged on the Rh complex via π - π - and $\text{C}=\text{O} \cdots \text{H}-\text{C}$ interactions.

Consequently, the reason for the low catalytic activity of RhphenPer under illumination is not associated with a slow protonation step but rather with the relatively slow formation of the fully reduced Rh^{I} center ($\text{Rh}^{\text{I}}\text{phenPer}$) in the solvent mixture used for the photocatalytic experiments (Figure S23) as after 10 min of irradiation only *ca.* 50% of all RhphenPer molecules did form $\text{Rh}^{\text{I}}\text{phenPer}$. We attribute this slow Rh^{I} formation under catalytic conditions to the rather short lifetime of the CS state. The overall photocatalytic efficiency is therefore very strongly affected by the apparent lower concentrations of TEA which is in acid base equilibrium with TEAH^+ because of buffering with NaH_2PO_4 to meet the pH needs for stabilizing NAD^+ .

Conclusion

We demonstrate a noble-metal free catalytically active molecular dyad using an organic photosensitizer (instead of transition metal-based chromophore) linked to a $[(\text{N}^{\wedge}\text{N})\text{Rh}(\text{Cp}^*)\text{Cl}]$ catalyst. The resultant photocatalyst $\text{Rh}^{\text{III}}\text{phenPer}$ consists of an organic **Per**-derived photosensitizing unit (**phenPer**) and a Rh^{III} catalytic center. Upon photoexcitation of $\text{Rh}^{\text{III}}\text{phenPer}$ charge is unidirectionally shifted towards the Rh center, forming a charge-separated species within *circa* 8 ps. In the absence of a sacrificial donor this species decays with *circa* 300 ps back to the ground state representing enhanced CS state lifetimes compared to other perylene dye-based transition metal complexes. In addition, RhphenPer could be used for formate-driven as well as light-driven NAD^+ co-factor reduction forming NADH with constant turnover frequencies. Compared to transition metal complex-based assemblies, the charge separation leading to pre-active species is likely still too short lived to enable higher light-driven catalytic activity. This needs to be approached in ongoing studies. However, since the properties of perylenes can be easily tuned by derivatization, increased charge separation distances as well as adjusted electrochemical and photophysical properties by incorporation of for example PMI and PDI systems need to be focused.

Experimental Section

The ligand **phenPer** was synthesized via Suzuki-Miyaura cross-coupling of 5-bromo-1,10-phenanthroline and 4,4,5,5-tetramethyl-2-(perylene-3-yl)-1,3,2-dioxaborolane^[45] (yield: 72%).^[45,46] For purification **phenPer** was re-crystallized in chloroform. The Rh^{III} complex, $[(\text{phenPer})\text{Rh}(\text{Cp}^*)\text{Cl}]\text{Cl}$ ($\text{Rh}^{\text{III}}\text{phenPer}$) was synthesized by reaction conditions adapted from literature.^[17] Purification was performed via size-exclusion chromatography. The compounds **phenPer** and $\text{Rh}^{\text{III}}\text{phenPer}$ were fully characterized by ^1H and ^{13}C NMR spectroscopy (see Figures S2–S5) as well as high-resolution mass spectrometry (see Figures S6 and S7).

The catalytic reactions were analyzed with UVvis absorption and emission spectroscopy. For thermal catalysis, 5 μM of the respective substance, 50 mM NaHCO_2 and 200 μM NAD^+ in 1:4 mixtures of acetonitrile and water were prepared in screw cap cuvettes. For light-driven reduction experiments, 5 μM of the respective substance, 0.1 M triethylamine (TEA) in 1:4 mixtures of acetonitrile and water were prepared in screw cap cuvettes. For light-driven catalysis, 5 μM of the respective substance, 0.12 M TEA and 0.1 M NaH_2PO_4 and 200 μM NAD^+ in 1:4 mixtures of acetonitrile and water were prepared in screw cap cuvettes. After a zero-point measurement, the cuvettes were transferred into a custom-made reactor equipped with cooling and LED illumination (400 nm with 14 mW cm^{-2} ; 470 nm with 50 mW cm^{-2}). After distinct time intervals, measurements by UVvis and emission spectroscopy were done.

The ultrafast transient absorption (fs-TA) spectra were collected upon 400 nm excitation. The setup is based on a Ti:Sapphire laser (Legend Elite, Coherent Inc.) yielding pulses centered at 795 nm (pulse-duration: 100 fs, repetition rate: 1 kHz). The 400 nm pump pulses were generated by second harmonic generation (BBO crystal). Those pulses were focused on the sample (1 mm cuvette) with an average intensity of 0.4 mW (gaussian beam profile of $400 \times 400 \mu\text{m}$). At the sample position the pump- and probe pulses are temporally and spatially overlapped in magic angle configuration. White-light was used as probe pulses, which was generated from the 795 nm fundamental laser pulses by focussing it on a rotating CaF_2 plate. Those probe pulses were temporally delayed with respect to the pump pulses by means of an optical delay stage (maximum delay of 2 ns). The probe pulses are split into two trains, namely a reference and probe path. Both pulses are focused on a diode array, directly (reference) or after the pulses were focused on the sample (probe). The probe pulses are recollimated and spectrally dispersed by a prism and detected by a diode array (Pascher Instruments AB, readout frequency of 1 kHz). The fs-TA data was analysed using the KiMoPack tool.^[47] Prior to global lifetime analysis the data was arrival-time corrected. The temporal resolution was limited to 0.3 ps, to avoid strong contributions of coherent artefacts to the signals.^[48,49] The pre-processed data was analysed using a parallel compartmental model (independent, first order decay employing three characteristic time-constants: $\Delta\text{Abs} = \sum_{i=1}^N a_i \cdot \exp(-k_i \cdot t)$). In this model, the three employed processes are associated with the so-called decay associated spectra (DAS), i.e., the exponential pre-factors (a_i). To model the additional deactivation channel, a target analysis was performed using KiMoPack, whereby the model as sketched in Figure 3, i.e., including an excited-state branching was employed. For both, global and target lifetime analysis, the errors of the fitted parameters (kinetic-rate constants) are obtained in a confidence level of 95%.

The quantum chemical calculations for investigating the structural and electronic properties of **phenPer** and $\text{Rh}^{\text{III}}\text{phenPer}$ were performed with the Gaussian 16 program.^[50] Initially, the angle between the perylene (**Per**) and phenanthroline (phen) moiety of

phenPer was scanned to find a fully relaxed equilibrium geometry of phenPer. That geometry was employed in the optimization of the structure of the respective Rh^{III} complex (Rh^{III}phenPer). The optimized singlet structures were obtained at the density functional level of theory (DFT) by means of the B3LYP XC functional.^[51,52] The def2-SVP basis^[53,54] as well as the respective core potentials (Rh) were applied for all atoms. A vibrational analysis was performed to verify that a minimum on the potential energy (hyper-)surface (PES) was obtained. The excited state properties, namely excitation energies, oscillator strengths and electronic characters were calculated within the Frack-Condon structure at the time-dependent DFT (TD-DFT) level of theory. Therefore, the 100 lowest singlet excited states were calculated using the same XC functional, basis set and core potentials as for the preceding ground state calculations. Solvent effects (acetonitrile, $\epsilon = 35.688$, $n = 1.344$) were taken into account on the ground and excited states properties by the solute electron density variant of the integral equation formalism of the polarizable continuum model.^[55,56] The non-equilibrium procedure of solvation was used for the calculation of the excitation energies within the Franck-Condon point. All calculations were performed including D3 dispersion correction with Becke-Johnson damping.^[57]

Acknowledgements

All authors gratefully acknowledge the German Science Foundation for funding via the TRR 234 CATALIGHT (project number 364549901, Project A1). J.B. is thankful for financial support by the Fonds der Chemischen Industrie (FCI) for a Kekulé-Stipendium. The authors thank the developers of the KIMOPACK software for the global lifetime analysis of the time-resolved spectra. All calculations were performed at the Universitätsrechenzentrum of the Friedrich Schiller University Jena. Open Access funding enabled and organized by Projekt DEAL.

Conflict of Interest

The authors declare no conflict of interest.

Data Availability Statement

The data that support the findings of this study are available from the corresponding author upon reasonable request.

Keywords: charge separation · perylene · photocatalysis · rhodium catalyst · time-resolved spectroscopy

- [1] C. Kranz, M. Wächter, *Chem. Soc. Rev.* **2021**, *50*, 1407–1437.
- [2] A. J. Esswein, D. G. Nocera, *Chem. Rev.* **2007**, *107*, 4022–4047.
- [3] G. Knör, *Coord. Chem. Rev.* **2015**, *304–305*, 102–108.
- [4] J. Roncali, *Chem. Rev.* **1992**, *92*, 711–738.
- [5] A. Mishra, C.-Q. Ma, P. Bäuerle, *Chem. Rev.* **2009**, *109*, 1141–1276.
- [6] F. Würthner, *Chem. Commun.* **2004**, 1564–1579.
- [7] T. Weil, T. Vosch, J. Hofkens, K. Peneva, K. Müllen, *Angew. Chem. Int. Ed.* **2010**, *49*, 9068–9093; *Angew. Chem.* **2010**, *122*, 9252–9278.
- [8] V. Kunz, V. Stepanenko, F. Würthner, *Chem. Commun.* **2015**, *51*, 290–293.
- [9] R. J. Lindquist, B. T. Phelan, A. Reynal, E. A. Margulies, L. E. Shoer, J. R. Durrant, M. R. Wasielewski, *J. Mater. Chem. A* **2016**, *4*, 2880–2893.

- [10] M. T. Vagnini, A. L. Smeigh, J. D. Blakemore, S. W. Eaton, N. D. Schley, F. D'Souza, R. H. Crabtree, G. W. Brudvig, D. T. Co, M. R. Wasielewski, *Proc. Nat. Acad. Sci.* **2012**, *109*, 15651–15656.
- [11] D. Costabel, A. Skabeev, A. Nabiyan, Y. Luo, J. B. Max, A. Rajagopal, D. Kowalczyk, B. Dietzek, M. Wächter, H. Görls, H. Görls, D. Ziegenbalg, Y. Zagranjarski, C. Streb, F. H. Schacher, K. Peneva, *Chem. Eur. J.* **2021**, *27*, 4081–4088.
- [12] N. T. La Porte, J. F. Martinez, S. Hedström, B. Rudshiteyn, B. T. Phelan, C. M. Mauck, R. M. Young, V. S. Batista, M. R. Wasielewski, *Chem. Sci.* **2017**, *8*, 3821–3831.
- [13] J. F. Martinez, N. T. La Porte, R. M. Young, A. Sinopoli, M. Sohail, M. R. Wasielewski, *J. Phys. Chem. C* **2019**, *123*, 6416–6426.
- [14] G. Knorr, D. Costabel, A. Skabeev, C. Neumann, J. Brossette, S. Kupfer, A. Turchanin, W. Weigand, K. Peneva, *Dye Pigment.* **2022**, *198*, 109940.
- [15] S. Fukuzumi, T. Kobayashi, T. Suenobu, *Angew. Chem.* **2011**, *123*, 754–757; *Angew. Chem. Int. Ed.* **2011**, *50*, 728–731.
- [16] U. Kölle, M. Grützel, *Angew. Chem. Int. Ed. Engl.* **1987**, *26*, 567–570.
- [17] A. K. Mengele, S. Kaufhold, C. Streb, S. Rau, *Dalton Trans.* **2016**, *45*, 6612–6618.
- [18] L. Zedler, A. K. Mengele, K. M. Ziems, Y. Zhang, M. Wächter, S. Gräfe, T. Pascher, S. Rau, S. Kupfer, B. Dietzek, *Angew. Chem. Int. Ed.* **2019**, *58*, 13140–13148; *Angew. Chem.* **2019**, *131*, 13274–13282.
- [19] K. T. Oppelt, J. Gasiorowski, D. A. M. Egbe, J. P. Kollender, M. Himmelsbach, A. W. Hassel, N. S. Sariciftci, G. Knör, *J. Am. Chem. Soc.* **2014**, *136*, 12721–12729.
- [20] L. Zedler, P. Wintergerst, A. K. Mengele, C. Müller, C. Li, B. Dietzek-Ivanšić, S. Rau, *Nat. Commun.* **2022**, *13*, 2538.
- [21] V. D. Parker, *J. Am. Chem. Soc.* **1976**, *98*, 98–103.
- [22] M. Ladwig, W. Kaim, *J. Organomet. Chem.* **1991**, *419*, 233–243.
- [23] B. S. Veldkamp, W.-S. Han, S. M. Dyar, S. W. Eaton, M. A. Ratner, M. R. Wasielewski, *Energy Environ. Sci.* **2013**, *6*, 1917.
- [24] G. W. Kinka, L. R. Faulkner, *J. Am. Chem. Soc.* **1976**, *98*, 3897–3901.
- [25] D. Casanova, *Int. J. Quantum Chem.* **2015**, *115*, 442–452.
- [26] M. Komfort, H.-G. Löhmansröben, T. Salthammer, *J. Photochem. Photobiol. A* **1990**, *51*, 215–227.
- [27] N. Mataga, T. Asahi, Y. Kanda, T. Okada, T. Kakitani, *Chem. Phys.* **1988**, *127*, 249–261.
- [28] C. R. Goldschmidt, M. Ottolenghi, *J. Phys. Chem.* **1971**, *75*, 3894–3897.
- [29] G. Angulo, A. Rosspeintner, B. Lang, E. Vauthey, *Phys. Chem. Chem. Phys.* **2018**, *20*, 25531–25546.
- [30] A. Aster, G. Licari, F. Zinna, E. Brun, T. Kumpulainen, E. Tajkhorshid, J. Lacour, E. Vauthey, *Chem. Sci.* **2019**, *10*, 10629–10639.
- [31] M. Hu, A. A. Sukhanov, X. Zhang, A. Elmali, J. Zhao, S. Ji, A. Karatay, V. K. Voronkova, *J. Phys. Chem. B* **2021**, *125*, 4187–4203.
- [32] S. J. Strickler, R. A. Berg, *J. Chem. Phys.* **1962**, *37*, 814–822.
- [33] K. H. Grellmann, A. R. Watkins, *Chem. Phys. Lett.* **1971**, *9*, 439–443.
- [34] K. Kawai, N. Yamamoto, H. Tsubomura, *Bull. Chem. Soc. Jpn.* **1970**, *43*, 2266–2268.
- [35] G. Sanna, M. I. Pilo, M. A. Zoroddu, R. Seeber, S. Mosca, *Inorg. Chim. Acta* **1993**, *208*, 153–158.
- [36] E. Lindsay, A. Vlcek, C. H. Langford, *Inorg. Chem.* **1993**, *32*, 2269–2275.
- [37] S. Zálaiš, C. Consani, A. El Nahhas, A. Cannizzo, M. Chergui, F. Hartl, A. Vlcek, *Inorg. Chim. Acta* **2011**, *374*, 578–585.
- [38] R. K. Dubey, M. Niemi, K. Kaunisto, K. Stranius, A. Efimov, N. V. Tkachenko, H. Lemmetyinen, *Inorg. Chem.* **2013**, *52*, 9761–9773.
- [39] C. L. Pitman, O. N. L. Finster, A. J. M. Miller, *Chem. Commun.* **2016**, *52*, 9105–9108.
- [40] Y. Peng, M. V. Ramos-Garcés, D. Lionetti, J. D. Blakemore, *Inorg. Chem.* **2017**, *56*, 10824–10831.
- [41] H. C. Lo, C. Leiva, O. Buriez, J. B. Kerr, M. M. Olmstead, R. H. Fish, *Inorg. Chem.* **2001**, *40*, 6705–6716.
- [42] K. E. Taylor, J. B. Jones, *J. Am. Chem. Soc.* **1976**, *98*, 5689–5694.
- [43] L. M. A. Quintana, S. I. Johnson, S. L. Corona, W. Villatoro, W. A. Goddard, M. K. Takase, D. G. VanderVelde, J. R. Winkler, H. B. Gray, J. D. Blakemore, *Proc. Nat. Acad. Sci.* **2016**, *113*, 6409–6414.
- [44] A. Marrone, R. H. Fish, *J. Organomet. Chem.* **2021**, *943*, 121810.
- [45] Y. Avlasevich, K. Müllen, *J. Org. Chem.* **2007**, *72*, 10243–10246.
- [46] D. S. Tyson, J. Bialecki, F. N. Castellano, *Chem. Commun.* **2000**, 2355–2356.
- [47] C. Müller, T. Pascher, A. Eriksson, P. Chabera, J. Uhlig, *J. Phys. Chem. A* **2022**, 10.1021/acs.jpca.2c00907.
- [48] B. Dietzek, T. Pascher, V. Sundström, A. Yartsev, *Laser Phys. Lett.* **2007**, *4*, 38–43.
- [49] A. L. Dobryakov, S. A. Kovalenko, N. P. Ernsting, *J. Chem. Phys.* **2005**, *123*, 044502.

- [50] M. J. Frisch, G. W. Trucks, H. B. Schlegel, G. E. Scuseria, M. A. Robb, D. J. Cheeseman, J. R. Scalmani, G. Barone, V. Petersson, G. A. Nakatsuji, H. Li, X. Caricato, M. Marenich, A. V. Bloino, J. Janesko, B. G. Gomperts, R. Mennucci, B. Hratchian, H. P. Ortiz, J. V. Izmaylov, A. F. Sonnenberg, J. L. Williams-Young, *Gaussian, Inc., Wallingford CT* **2016**.
- [51] A. D. Becke, *J. Chem. Phys.* **1993**, *98*, 5648–5652.
- [52] C. Lee, W. Yang, R. G. Parr, *Phys. Rev. B* **1988**, *37*, 785–789.
- [53] F. Weigend, R. Ahlrichs, *Phys. Chem. Chem. Phys.* **2005**, *7*, 3297.
- [54] F. Weigend, *Phys. Chem. Chem. Phys.* **2006**, *8*, 1057.
- [55] B. Mennucci, C. Cappelli, C. A. Guido, R. Cammi, J. Tomasi, *J. Phys. Chem. A* **2009**, *113*, 3009–3020.
- [56] A. V. Marenich, C. J. Cramer, D. G. Truhlar, *J. Phys. Chem. B* **2009**, *113*, 6378–6396.
- [57] S. Grimme, S. Ehrlich, L. Goerigk, *J. Comput. Chem.* **2011**, *32*, 1456–1465.

Manuscript received: June 22, 2022
Accepted manuscript online: August 3, 2022
Version of record online: September 2, 2022